Equilibria and Rate Phenomena from Atomistic to Meso-scale: Simulation Studies of Magnetite

Christianna N. Lininger[a], *Nicholas W. Brady*[a], *Alan C. West*[a,b,*]

[a] Department of Chemical Engineering, Columbia University, New York, NY 10027, United States

[b] Department of Earth and Environmental Engineering, Columbia University, New York, NY 10027, United States

*Email: acw7@columbia.edu

CONSPECTUS

Batteries are dynamic devices comprised of multiple components that operate far from equilibrium and may operate under extreme stress and varying loads. Studies of isolated battery components are valuable to the fundamental understanding of the physical processes occurring within each constituent element. When the components are integrated into a full device and operated under realistic conditions, it can be difficult to decouple the physical processes that occur across multiple interfaces and multiple length scales. Thus, the physical processes studied in isolated components may change in a full battery setup or may be irrelevant to performance. Simulation studies on many length scales play a key role in the analysis of experiments and in the elucidation of the relevant physical processes.

In this review, we aim to highlight the use of modeling on multiple length scales to identify rate limiting phenomena in lithium-ion batteries. To illustrate the utility of modeling, we examine lithium-ion batteries with nanostructured magnetite, Fe_3O_4, as the positive electrode active material against a solid Li^0 negative electrode. Due to continuous operation away from equilibrium, batteries exhibit highly non-ideal behavior, and a model that aims to reproduce behavior under realistic operating conditions must be able to capture the physics occurring on the length scales relevant to the performance of the system. It is our experience that limiting behavior in lithium-ion batteries can be observed on the atomic scale and up through the electrode scale and thus, predictive models must be capable of integrating and communicating physics across multiple length scales.

Magnetite is studied as an electrode material for lithium-ion batteries, but it is found to suffer from slow solid-state transport of lithium, slow reaction kinetics, and poor cycling.

Magnetite (Fe_3O_4) is a material capable of undergoing multiple electron transfers (MET), and can accept up to 8 lithium per formula unit ($Li_8Fe_3O_4$). Magnetite, $(Fe_{8a}^{3+})[Fe^{3+}Fe^{2+}]_{16d}O_{4,32e}^{2-}$, has a close-packed inverse spinel structure and undergoes both intercalation and conversion reactions upon full lithiation.[1] To overcome solid-state transport resistances, magnetite can be nanostructured to decrease Li^+ diffusion lengths, and this has been shown to increase capacity. Additionally, unique architectures incorporating both carbon and Fe_3O_4 have shown to alleviate transport and cycling issues in the material.[2] Here, we solely address traditional composite electrodes, in which Fe_3O_4 is synthesized as nanoparticles and combined with additives to fabricate the electrode.

In the case of nanoparticulate magnetite, it has been found that the electrode fabrication process results in the formation of micron-sized agglomerates of the Fe_3O_4 nanoparticles, introducing a secondary structural motif. The agglomerates may form in one or more fabrication processes, and their elimination may not be straightforward or warranted. Here, we highlight the impact of these secondary formations on the performance of the Fe_3O_4 lithium-ion battery. We illustrate how simulations can be used to design experiments, prioritize research efforts, and predict performance.

1. INTRODUCTION

Lithium-ion chemical energy storage affects daily life, enabling the portability of both consumer and professional devices, and will be key in the large-scale deployment of electric vehicles. Individual battery cells can be combined to create a multi-cell configuration; the optimization of cell packs is an engineering-design problem that factors in cost and safety and other physical constraints. The cell scale (Figure 1a) is the most basic battery unit. This is where

most of the chemistry and physics of the technology can be studied and where materials innovation and development are most active. Fundamental research of the phenomena occurring at interfaces and across multiple length scales can propel developments that reduce the cost, extend the life, improve the safety and performance of batteries, and may enable full penetration into transportation and grid-scale markets.

(Insert Figure 1)

Lithium-ion batteries store and release energy by conversion between chemical potential and electrical work. The main components of a lithium battery are the anode (negative electrode), cathode (positive electrode), separator, and the electrolyte, as depicted in Figure 1a. During discharge, chemical energy stored in the battery is released as electrical energy. A solid lithium negative electrode is shown, but other chemistries, such as lithium-graphite, are more commonly used in commercial batteries. At the negative electrode, lithium is oxidized, producing free electrons and mobile lithium ions. From the negative electrode, the electrons travel through a load, and the lithium ions travel through the electrolyte towards the positive electrode where they react with the active material (Figure 1a). Inverse spinel (Fd3m) magnetite, $(Fe_{8a}^{3+})[Fe^{3+}Fe^{2+}]_{16d}O_{4,32e}^{2-}$, is an active material with a high theoretical capacity (926 mAhg^{-1}), due to its ability to accommodate eight lithium atoms per formula unit ($Li_8Fe_3O_4$). Magnetite has been studied as a positive electrode material since the 1980s, both experimentally[3] and theoretically,[4] and as a result much is known about how the material accepts lithium. At low lithium concentrations, there is an intercalation regime followed by a phase change that proceeds with slow kinetics. At high lithium concentrations, conversion to $Li_2O + Fe^0$ is observed.[3–5] The average solid-state lithium concentration at which these processes are observed is a function of particle size and discharge rate.[6,7] Due to slow kinetics, particle-size dependence, and

irreversibilities during cycling, the realized capacity can be significantly lower than the theoretical maximum.

To mitigate the solid-state transport resistances, magnetite is nanostructured, which can lead to the formation of secondary structures such as the agglomerates of nanoparticles observed in Figure 1b and 1c.[8–10] Bulk or idealized experiments may not represent what occurs when multiple interfaces are introduced, such as the interfaces between nanoparticles, additives, and the electrolyte, or interfaces that form from nanoparticle agglomeration (Figure 1d). However, from the perspective of modeling, interfaces allow for the system to be segregated into well-defined regions, enabling the identification of bottlenecks - the component(s) and length scales that significantly impact performance.

2. MECHANISTIC & ATOMIC SCALE STUDIES OF MAGNETITE

2.1 Mechanistic Understanding of the Reversible Potential

Pioneering work on the lithiation of magnetite was conducted by Thackeray, David, and Goodenough in 1982. Thackeray *et al.* conducted open circuit measurements in conjunction with powder X-ray diffraction measurements of <44 μm Fe_3O_4 particles. Measurements performed 24 hours after lithiation were used to elucidate the reaction mechanisms occurring during lithiation of magnetite (Figure 2).[3] Thackeray *et al.* reported that initial lithium insertion into magnetite, $(Fe_{8a}^{3+})[Fe^{3+}Fe^{2+}]_{16d}O_{4,32e}^{2-}$ (Figure 2a), produced a defective rocksalt, $[Li^{+}Fe^{2+}]_{16c}[Fe^{3+}Fe^{2+}]_{16d}O_{4,32e}^{2-}$, (Figure 2d). The authors hypothesized that lithium inserted onto vacant 16c sites until a critical concentration was reached, where Coulombic repulsion between lithium in 16c sites and iron in the nearby tetrahedral 8a sites caused the tetrahedral 8a iron to move to vacant octahedral 16c sites (Figures 2b and 2c). Lithiation past $x = 1.0$ resulted in

lithium insertion into vacant tetrahedral sites, $(Li^{+})_{8a/8b/48f}[Li^{+}Fe^{2+}]_{16c}[Fe^{2+}Fe^{2+}]_{16d}O^{2-}_{4,32e}$. Full lithiation to 8 equivalents resulted in conversion to Li_2O + Fe^0.[3] The first theoretical investigation of lithium insertion into Fe_3O_4 was carried out by Islam and Catlow in 1988.[4] They used interatomic potentials to model host-host and host-intercalate ion interactions and validated Thackeray *et al.*'s findings that lithium preferentially occupies vacant octahedral sites over tetrahedral sites, and that lithium insertion resulted in the displacement of tetrahedral 8a iron.[3,4]

(Insert Figure 2)

In a subsequent review in 1987 by Thackeray *et al.*, a more refined reversible potential was reported. Two plateaus were observed, the first originating at x = 1.0 and a potential of 1.2 V, for which the products could not be determined from powder XRD due to poor crystallinity. The second plateau occurred from x = 1.5 through full lithiation, believed to be the conversion to Li_2O + Fe^0.[11] Both of the reversible potentials in the literature reported by Thackeray *et al.* are reproduced in Figure 3b. In 2015, Knehr *et al.* reported the voltage relaxation for 6, 8, and 32-nm Fe_3O_4 particles and resultant reversible potential for lithiation into 6 and 8-nm Fe_3O_4 particles, using the resting voltage 30 days after lithiation. The 6, 8, and 32-nm particles undergo two voltage plateaus, the first at ~1.8 V and the second at ~1.2 V (Figure 3a).[12]

(Insert Figure 3)

Reversible potentials can be estimated from first principles with Density Functional Theory (DFT) calculations.[13–15] To accurately capture the electronic and magnetic properties in magnetite, the electron correlation in the *d* orbitals of iron must be accounted for with the Hubbard U correction.[16,17] DFT+U voltages are calculated from periodically repeating structures representative of bulk materials at 0 K and 0 pressure. Guided by the stable phases on the ternary

Li-Fe-O phase diagram, He *et al.* used DFT+U calculations to predict the reversible potential of lithium insertion into bulk magnetite over the full range of lithiation, $0 < x < 8$ (Figure 3d).[7] However, from Figures 3a and 3b it appears that the observed reversible potential varies as a function of magnetite particle size. This indicates that although the DFT+U studies can give insight into possible reactions occurring in a bulk material, models and first principles methods that capture the effects of nanosizing may be necessary for a full understanding of the thermodynamics of magnetite. For example, surface non-idealities in magnetite may be important, and would be especially impactful as nanoparticle size decreases.

2.2 Observations of Phase Change

At the atomic length scale, the insertion of lithium into host materials can cause phase change by inducing movement of the iron atoms. The slope of the reversible potential can be used to suggest when two phases are in equilibrium, while materials characterization methods allow for equilibrium phase identification.[18,19] The reversible potential for full discharge ($0 < x < 8$) of 8-nm magnetite shows two flat voltage plateaus ($1 < x < 2.5$ and $5\text{-}6 < x < 8$), suggesting two phase changes, as seen in Figure 3a. However, magnetite has slow phase-change kinetics, so during discharge a voltage plateau may be difficult to observe, making it challenging to rely on only electrochemical measurements to identify the formation of a new phase.

Using *in situ* TEM, He *et al.* observed multiple phases in a single 80-nm nanoparticle, due to the occurrence of simultaneous reactions.[7] Bock *et al.* also observed particle phase inhomogeneity and studied the effect of particle size on the kinetics of phase change. Bock *et al.* used *in situ* XRD and *ex situ* XAS on 11-nm and 39-nm magnetite particles, and found that the mechanism of the first intercalation process, $0 < x < 1.0$, was independent of particle size. However, the mechanisms for lithiation beyond $x = 1$, that involved the Fe^0 conversion process,

appeared to be crystallite-size dependent.[6] In Figure 4a, which is adapted from Abraham *et al*., the results of various studies are summarized as a function of lithium concentration in 9-10.6 nm Fe_3O_4 particles.[1] The X-ray Diffraction (XRD) data[20] in the first column is a measure of the averaged long-range order in a sample, while the next four columns[5] give structurally refined information concerning local chemical environments. Possible discrepancies within Figure 4a and with other studies may be attributed, in part, to the significant spatial variations in lithiation state, i.e. the phase inhomogeneity observed experimentally in single particles.

(Insert Figure 4)

To probe the observation of phase inhomogeneity in lithiated magnetite nanoparticles, a validated model was used to predict the maximum lithium concentrations, x_{max}, as a function of the measured discharged concentration in Figure 4b.[12,21] The model is standard porous electrode theory, discussed in detail in Section 3, and a graphic of the electrochemical system being modeled can be seen in Figure 1. The system was comprised of nanoparticulate Fe_3O_4, that was observed to aggregate into micron-sized agglomerates upon electrode fabrication. The model predicted voltage profiles as a function of the measured discharged lithium concentration. The simulated voltage profiles were validated against experimental voltage profiles for two systems comprised of two different active material nanoparticle sizes, 8 nm and 32 nm. Following model validation against electrochemical data, the model was used to predicted concentration profiles occurring in single crystals in the system and in the secondary micron-sized aggregates.

The simulation predicts that the 32-nm particles undergo much higher local lithium concentrations than the 8-nm particles at the same depth of discharge. As seen in Figure 4b, when $x \sim 0.75$ equivalents of lithium have been discharged in a system comprised of agglomerated 32-

nm magnetite particles, the local Li concentrations are predicted to be as high as $x \sim 6.0$. When this same concentration, $x \sim 0.75$, is discharged in a system comprised of agglomerated 8-nm particles, the maximum local Li concentrations are less than 3.0. At 6.0 equivalents, the conversion reaction to $Li_2O + Fe^0$ is expected to occur, but at concentrations less than 3.0 equivalents, a FeO-like phase or composite $FeO{\cdot}Li_2O$ have been observed.[1,5,6] These local increased concentrations result from transport resistances on both the agglomerate-scale and the crystal-scale. This is commensurate with Bock *et al.'s* observation that the larger particles, with larger Li^+ diffusion lengths (higher solid-state transport resistances), converted to $Li_2O + Fe^0$ at lower average lithium concentrations than the smaller particles, presumably because of higher localized solid-state Li concentrations.[6] The simulation predictions allow for a reconciliation of the observation of phase inhomogeneity within the crystals, and how the inhomogeneities change as a function of crystal size.

2.3 Cycling and Dynamic Behavior

Capacity fade can indicate irreversibilities, including side reactions which may be especially important in the first cycle when the solid-electrolyte interface (SEI) is formed. Irreversibilities can arise from many factors including irreversible phase change, mechanical stress, and surface modification of the active material.[22,23] In practice, the first cycle may be engineered to result in irreversible SEI formation that prolongs the life of the battery. Using cyclic voltammetry on magnetite, one study found significant differences between the first discharge cycle and all subsequent cycles.[24] Namely, the first discharge showed three peaks corresponding to three distinct mechanisms of lithium insertion into magnetite: lithium insertion into octahedral sites, shifting of tetrahedral iron to octahedral sites, and conversion to $Li_2O + Fe^0$ (which occurs in parallel to lithium insertion into carbon). However, the second and subsequent discharge cycles

only show one reduction peak, attributed primarily to the $3FeO + 6\ Li^+ + 6\ e^- \rightarrow 3Fe^0 + 3Li_2O$ conversion reaction.[24] In another cycling study, following full lithiation to $Li_8Fe_3O_4$, delithiation was unable to extract all of the inserted lithium, and the material failed after four cycles.[25] The inability to extract all inserted lithium suggests an irreversible phase change may arise at some point between $0 < x < 8$. Komaba *et al.* found that 10-nm and 100-nm magnetite particles were shown to cycle without substantial fade for up to 25 cycles if the material was only discharged to $x < 2$. However, Komaba *et al.* found that 400-nm magnetite particles cycled poorly compared to the 10 and 100-nm.[8]

3. CONTINUUM MODELING OF MAGNETITE

3.1 Introduction to Mathematical Modeling of Magnetite

Physics-based cell modeling on the macroscopic scale can involve the optimization of several parameters: electrode thickness, pore size, active materials ratios, and particle size. More complex modeling can incorporate microscopic descriptions, such as the inclusion of meso length scales within an electrode, and descriptions of interfaces that result from the creation of porous pathways, as opposed to single geometric corrections for tortuosity.[26,27] A model was developed by Knehr *et al.* for an electrode comprised of nanoparticulate magnetite that aggregated into micron-sized agglomerates. In addition to Butler-Volmer electrochemical kinetics, and phase change reactions, the model incorporated transport of lithium in the solid-state (on the nanocrystal-scale) and transport of Li-ions on the agglomerate-scale, i.e. through the pores between nanoparticles.[12,21,28] Predictions from this model have identified major resistances associated with different interfaces and length scales, and these are discussed in the following sections alongside a discussion of the model development.

3.2 The Reversible Potential in Mathematical Based Models

To incorporate Butler-Volmer electrochemical kinetics into a mathematical model, there must first be a description of the thermodynamics, primarily in the form of a reversible potential as a function of state of (dis)charge. For some systems, a thermodynamic treatment of phase equilibria may also be required. Solid-state redox reactions are characteristic processes of intercalation reactions, and during these processes the equilibrium potential deviates significantly from Nernstian behavior.[29,30] Because of these deviations, many corrections to the Nernst potential have been proposed – namely, activity coefficient corrections such as one- and two-parameter Margules relations, and Redlich-Kister equations.[31–33] For the case of lithium insertion into magnetite, Knehr *et al.* used a Redlich-Kister equation to develop an expression for the reversible potential by fitting experimental data from voltage recovery experiments of 6, 8, and 32-nm particles, Figure 3a and 3c.[12,28] The empirical fit resembles the experimental data, but does not always provide physical intuition or insight. Simulation results from mathematical-based models are highly sensitive to the description of the reversible potential, and the models require a continuous and numerically accurate reversible potential. A primary utility of the mathematical model is in describing the rate phenomena such as electrochemical reactions and transport. Considering the empirical nature of the fitting of the reversible potential to data, a good continuum-level model is predictive of the *deviation* from the reversible potential.

3.3 Modeling of Ionic Transport

Galvanostatic Intermittent Titration Technique (GITT) experiments are often used to estimate mass-transfer resistances (diffusion coefficients), taking advantage of the very different characteristic time scales for mass-transfer compared to other system impedances. However, a straightforward theory used for interpretation may not be easily applicable to all positive electrode materials.[34] Nevertheless, GITT experiments are often used to derive an effective chemical

diffusion coefficient.[34,35] Deploying a detailed mathematical model based on porous electrode theory, Knehr *et al.* used the relaxation portion of GITT experiments to isolate transport processes from charge-transfer effects.[12] The observed relaxation times were too large (> 100 hours) to be attributed to electrode-scale mass-transfer using any reasonable estimate of the diffusion coefficient of Li-ions in the electrolyte,[12] so models were developed on the crystal and agglomerate length scales. The crystal-scale model described the transport of lithium within the nanocrystal solid-state magnetite structure, Figure 1e. The agglomerate-scale model described the transport of lithium ions (Li^+ in the electrolyte) moving through the porous spaces between nanoparticles within the agglomerate, Figure 1d.[12,21]

For small particle sizes, 6-nm and 8-nm, the agglomerate-scale model accurately captured both discharge and voltage recovery measurements, while the crystal-scale model could not accurately capture both of these observations with a consistent set of physical parameters. For a larger crystal size, 32-nm, it was found that there was an additional resistance, hypothesized to be associated with transport within the larger crystals. Crystal-scale mass transfer resistances were apparently negligible in crystals smaller than 10-nm at the studied discharge rate. To reconcile these two findings, a multi-scale crystal and agglomerate model was developed that included transport on the crystal-scale and the transport of lithium through the porous regions between the nanoparticles on the agglomerate-scale (Figures 1d and 1e). It was found that only the inclusion of both crystal-scale and agglomerate-scale effects could describe both discharge and relaxation for 6, 8, and 32-nm systems.[12,21]

(Insert Figure 5)

The findings indicated that for a 32-nm crystal, transport on both the agglomerate and crystal scales significantly impact performance. In Figure 5, the blue curve shows a very significant deviation from the reversible potential due to the combination of both agglomerate-scale and crystal-scale resistances. The red curve shows the expected performance if the agglomerate-scale resistances were eliminated. Because of the slow transport of lithium, both through the solid-state as well as through the agglomerate, crystal-scale and agglomerate-scale effects both contribute significantly to performance losses. It was estimated that the solid-state diffusion coefficient in the crystal was 2.0 x 10^{-18} cm^2 s^{-1}, which is in the lowest range of mobilities in candidate intercalation materials.[36] The model-derived solid-state diffusion coefficient is an effective diffusivity of lithium in crystalline magnetite. The actual diffusion coefficient likely varies with lithium concentration. The diffusion coefficient for Li within the agglomerate was 2.3 x 10^{-13} cm^2 s^{-1}, which is very low compared to what would be expected from common approximations that account for porosity and tortuosity while assuming that Li-electrolyte frictional interactions remain unchanged from a bulk electrolyte, on the order of 10-6 cm^2 s^{-1}.[37,38] This result indicates that the simplified geometric correction is insufficient to capture the physics occurring in the system. They interpret that this is because the void space between nanoparticles is sufficiently small that solution-surface frictional interactions (i.e. surface diffusion) are more important to mobility than solute-solvent interactions. Adsorption and migration of various chemical species, including lithium, on the surfaces of magnetite is well studied in environments relevant to catalysis.[39–41] However, quantifying the adsorption and surface migration of lithium on the magnetite nanoparticle surfaces in a lithium-ion battery is complicated by the known occurrence of surface layers.[24,42]

3.4 Mathematical Modeling of Phase Change

Characterization of magnetite during (de)lithiation reveals that the material undergoes intercalation reactions initially, while at higher concentrations of lithium, conversion reactions are observed.[5] The previously discussed model, which incorporated Butler-Volmer electrochemical kinetics as well as transport on the crystal and agglomerate length scales, was able to accurately capture the observed performance at low levels of lithiation as well as the initial voltage relaxation performance (< 200 hours). However, at high levels of lithiation, without the inclusion of phase change in the model, the simulated and observed voltage relaxation profiles differed at long times (> 500 hours). For instance, at long times, the voltage relaxation curves continuously increase over the course of 80+ hours, where a model without phase change predicts a plateau.[28]

To introduce phase change, a kinetic model inspired by the Avrami theory for nucleation and growth was used to describe the phase transformation kinetics associated with three distinct materials – α-$Li_xFe_3O_4$, β-$Li_4Fe_3O_4$ and γ-(Li_2O + Fe^0). The chemical structure of these materials is not specified or necessary to implement the mathematical model, but rather the model addresses the averaged lithium concentration and the kinetics of phase change. Inclusion of these phase change processes improved agreement with electrochemical experiments for higher lithium concentrations and also accurately simulated the end of relaxation voltages. It was determined that transformation from α to β proceeds slowly and can be observed in the relaxation profiles as the slow continuous voltage increase over long times. It was also found that the transition of α to γ proceeds quickly, reconciling the observation of inhomogeneity and more extensive Li_2O + Fe^0 formation in larger particles.[28]

The introduction of kinetic models for phase change provides significant practical advantages over formulations that are based on a phase equilibrium between the two phases because it is easier to implement numerically, is more general, and yet can still replicate a

shrinking-core model through adjustment of model parameters. In short, the method simplifies the process of tracking the movement of multiple phase boundaries. With other methods, specific infrastructure needs to be developed within the software to manage the movement and coalescence of interfaces.[28,43]

4. DESIGN & OPTIMIZATION

Numerical simulations are an almost indispensable tool for analysis of electrochemical characterization of batteries and battery materials, especially when coupled to materials characterization over multiple time and length scales. They are commonly used for design of systems, for example, an optimal positive to negative electrode mass ratio for a given application. They can also be deployed for more basic studies, not only to design experimental protocols but to focus experimental efforts towards material synthesis/discovery that may have the greatest impact on performance.

For magnetite, model predictions suggest that agglomerate-scale transport impedances have a large impact on electrochemical performance.[12,21] Bock *et al.* employed a nanoparticle surface capping method to minimize aggregation of the nanoparticulate magnetite to further probe the effects of agglomeration.[24] Electrochemical measurements showed that the dispersed samples (*i.e.* no agglomerates) had improved performance in the initial cycles but showed continuous capacity fade with cycling, while aggregated samples retained > 95% of their initial capacity.[24] Bock *et al.'s* experimental study suggested that the elimination of agglomerates allowed more surface area in the active material to be accessible to charge transfer by reducing transport resistances through the agglomerates. However, the dispersed particles cycled more poorly than the aggregated samples. Thus, there may exist an ideal combination of agglomerate and crystal sizes.

(Insert Figure 6)

Assuming aggregation may improve cycling, one can ask if there is an optimal size such that the agglomerates are made sufficiently small to avoid transport impedances while being large enough to stabilize the electrode. While we are not able to simulate or explain any potential stabilizing effect, simulations allow for facile evaluation of the agglomerate-scale impedances. Likewise, simulations allow for evaluation of the impact of reducing crystal-scale, considering not only reduction in solid-state transport resistances but losses of active materials associated with SEI formation. We have simulated the overpotential at x = 1.5 for C/200 discharge as a function of nanoparticle and agglomerate sizes. As can be seen in Figure 6, there are crystal-scale effects, where larger crystals have higher overpotentials due to solid-state transport. However, efforts to decrease crystal sizes from 10-nm to 6-nm do not yield a significant decrease in overpotential. For agglomerates between 0.1 and 0.5 microns, the transport resistances associated with the agglomerate-scale are not significant compared to the overall impedance for crystallite sizes. However, electrodes with agglomerates larger than 0.5 microns show significant reduction in performance. The simulations suggest that there exists a minimum agglomerate size, below which performance is not impacted. However, this minimum size should be a strong function of rate. Nevertheless, such concepts can be exploited if agglomeration does stabilize cycling behavior.

5. CONCLUDING REMARKS

Batteries remain relevant technological devices impacting everyday life from portable electronics to the future implementation into grid-storage and electric vehicle markets. Introduction of constituent materials into the device introduces complexities including interfaces, and this necessitates understanding on multiple length and time scales. Fundamental studies of magnetite have shown slow phase change upon lithiation and significant solid-state transport

resistances. Fabrication of the composite electrode induces agglomeration of the Fe_3O_4 nanoparticles into secondary micron sized motifs, and these features impact device performance. Simulations, closely coupled to experiment, enable identification of rate-limiting processes occurring over varying interfaces and length scales. The ability to identify the resistance on all length scales and to predict their effect on performance is imperative to the design and realization of the next generation of lithium-ion batteries.

Acknowledgements:

C. N. L. and N. W. B. contributed equally to this work. This work was supported as part of the Center for Mesoscale Transport Properties, an Energy Frontier Research Center supported by the U.S. Department of Energy (DOE), Office of Science, Basic Energy Sciences, under Award DE-SC0012673. C. N. L. acknowledges the support of the National Science Foundation Graduate Research Fellowship under Grant No. 1644869. Any opinions, findings, and conclusions or recommendations expressed in this material are those of the authors and do not necessarily reflect the views of the National Science Foundation. We acknowledge computing resources from Columbia University's Shared Research Computing Facility project, which is supported by NIH Research Facility Improvement Grant 1G20RR030893-01, and associated funds from the New York State Empire State Development, Division of Science Technology and Innovation (NYSTAR) Contract C090171, both awarded April 15, 2010.

BIOGRAPHICAL INFORMATION

Alan West received his PhD in Chemical Engineering from the University of California at Berkeley and his BS from Case Western Reserve University. He is the current chair of the Department of Chemical Engineering at Columbia University and is the Samuel Ruben-Peter G. Viele Professor of Electrochemistry. His research interests include electrochemical

microfabrication methods, electrochemical sensors, batteries, bioelectrochemical synthesis, and fuel cells.

Date of Birth: 06/02/1963

Christianna Lininger is a PhD candidate in Alan West's group in the Department of Chemical Engineering at Columbia University and is a 2014 NSF GRFP Fellow. She received her BS at the University of California at San Diego in chemical engineering with an area of specialization in nanoengineering. She currently utilizes density functional theory calculations to study the atomistic processes occurring upon lithiation of active materials for lithium-ion batteries.

Date of Birth: 04/21/1988

Nicholas Brady is a PhD candidate in Alan West's group in the Department of Chemical Engineering at Columbia University. He received his BS at the University of California, Berkeley in chemical engineering with a joint-major in material science and engineering. Nick uses continuum simulations to interrogate the physics of lithium insertion in candidate cathode materials.

Date of Birth: 12/06/1990

References:

(1) Abraham, A.; Housel, L. M.; Lininger, C. N.; Bock, D. C.; Jou, J.; Wang, F.; West, A. C.; Marschilok, A. C.; Takeuchi, K. J.; Takeuchi, E. S. Investigating the Complex Chemistry of Functional Energy Storage Systems: The Need for an Integrative, Multiscale (Molecular to Mesoscale) Perspective. *ACS Cent. Sci.* **2016**, *387*, 380–387.

(2) Zhou, G.; Wang, D.-W.; Li, F.; Zhang, L.; Li, N.; Wu, Z.-S.; Wen, L.; Lu, G. Q. (Max); Cheng, H.-M. Graphene-Wrapped Fe3O4 Anode Material with Improved Reversible Capacity and Cyclic

Stability for Lithium Ion Batteries. *Chem. Mater.* **2010**, *22*, 5306–5313.

(3) Thackeray, M. M.; David, W. I. F.; Goodenough, J. B. Structrural Characterization of the Lithiated Iron Oxides LixFe3O4 and LixFe2O3 (0<x<2). *Mater. Res. Bull.* **1982**, *17*, 785–793.

(4) Islam, M. S.; Catlow, C. R. A. Lithium Insertion into Fe304. *J. Solid State Chem.* **1988**, *77*, 180–189.

(5) Zhang, W.; Bock, D. C.; Pelliccione, C. J.; Li, Y.; Wu, L.; Zhu, Y.; Marschilok, A. C.; Takeuchi, E. S.; Takeuchi, K. J.; Wang, F. Insights into Ionic Transport and Structural Changes in Magnetite during Multiple-Electron Transfer Reactions. *Adv. Energy Mater.* **2016**, *6*.

(6) Bock, D. C.; Pelliccione, C. J.; Zhang, W.; Timoshenko, J.; Knehr, K. W.; West, A. C.; Wang, F.; Li, Y.; Frenkel, A. I.; Takeuchi, E. S.; Takeuchi, K. J.; Marschilok, A. C. Size Dependent Behavior of Fe3O4 Crystals during Electrochemical (De)lithiation: An in Situ X-Ray Diffraction, Ex Situ X-Ray Absorption Spectroscopy, Transmission Electron Microscopy and Theoretical Investigation. *Phys. Chem. Chem. Phys.* **2017**, *19*, 20867–20880.

(7) He, K.; Zhang, S.; Li, J.; Yu, X.; Meng, Q.; Zhu, Y.; Hu, E.; Sun, K.; Yun, H.; Yang, X.-Q.; Zhu, Y.; Gan, H.; Mo, Y.; Stach, E. A.; Murray, C. B.; Su, D. Visualizing Non-Equilibrium Lithiation of Spinel Oxide via in Situ Transmission Electron Microscopy. *Nat. Commun.* **2016**, *7*, 11441.

(8) Komaba, S.; Mikumo, T.; Yabuuchi, N.; Ogata, A.; Yoshida, H.; Yamada, Y. Electrochemical Insertion of Li and Na Ions into Nanocrystalline Fe3O4 and α-Fe2O3 for Rechargeable Batteries. *J. Electrochem. Soc.* **2010**, *157*, A60.

(9) Zhu, S.; Marschilok, A. C.; Takeuchi, E. S.; Takeuchi, K. J. Crystallite Size Control and Resulting Electrochemistry of Magnetite, Fe3O4. *Electrochem. Solid-State Lett.* **2009**, *12*, A91.

(10) Bock, D. C.; Kirshenbaum, K. C.; Wang, J.; Zhang, W.; Wang, F.; Wang, J.; Marschilok, A. C.; Takeuchi, K. J.; Takeuchi, E. S. 2D Cross Sectional Analysis and Associated Electrochemistry of Composite Electrodes Containing Dispersed Agglomerates of Nanocrystalline Magnetite, Fe3O4. *ACS Appl. Mater. Interfaces* **2015**, *7*, 13457–13466.

(11) Thackeray, M. M.; de Picciotto, L. A.; de Kock, A.; Johnson, P. J.; Nicholas, V. A.; Adendorff, K.

T. Spinel Electrodes for Lithium Batteries - A Review. *J. Power Sources* **1987**, *21*, 1–8.

(12) Knehr, K. W.; Brady, N. W.; Lininger, C. N.; Cama, C. A.; Bock, D. C.; Lin, Z.; Marschilok, A. C.; Takeuchi, K. J.; Takeuchi, E. S.; West, A. C. Mesoscale Transport in Magnetite Electrodes for Lithium-Ion Batteries. *ECS Trans.* **2015**, *69*, 7–19.

(13) Ceder, G.; Aydinol, M. K.; Kohan, A. F. Application of First-Principles Calculations to the Design of Rechargeable Li Batteries. *Comput. Mater. Sci.* **1997**, *8*, 161–169.

(14) Benco, L.; Barras, J.-L.; Atanasov, M.; Daul, C. A.; Deiss, E. First-Principles Prediction of Voltages of Lithiated Oxides for Lithium-Ion Batteries. *Solid State Ionics* **1998**, *112*, 255–259.

(15) Urban, A.; Seo, D.-H.; Ceder, G. Computational Understanding of Li-Ion Batteries. *npj Comput. Mater.* **2016**, *2*, 16002.

(16) Anisimov, V. I.; Aryasetiawan, F.; Lichtenstein, A. I. First-Principles Calculations of the Electronic Structure and Spectra of Strongly Correlated Systems: The LDA + U Method. *J. Phys. Condens. Matter* **1997**, *9*, 767–808.

(17) Wang, L.; Maxisch, T.; Ceder, G. Oxidation Energies of Transition Metal Oxides within the GGA+U Framework. *Phys. Rev. B - Condens. Matter Mater. Phys.* **2006**, *73*, 1–6.

(18) Liu, X.; Wang, D.; Liu, G.; Srinivasan, V.; Liu, Z.; Hussain, Z.; Yang, W. Distinct Charge Dynamics in Battery Electrodes Revealed by in Situ and Operando Soft X-Ray Spectroscopy. *Nat. Commun.* **2013**, *4*, 1–8.

(19) Ceder, G.; Ven, A. Van Der. Phase Diagrams of Lithium Transition Metal Oxides : Investigations from First Principles. *Electrochim. Acta* **1999**, *45*, 131–150.

(20) Menard, M. C.; Takeuchi, K. J.; Marschilok, A. C.; Takeuchi, E. S. Electrochemical Discharge of Nanocrystalline Magnetite: Structure Analysis Using X-Ray Diffraction and X-Ray Absorption Spectroscopy. *Phys. Chem. Chem. Phys.* **2013**, *15*, 18539.

(21) Knehr, K. W.; Brady, N. W.; Cama, C. A.; Bock, D. C.; Lin, Z.; Lininger, C. N.; Marschilok, A. C.; Takeuchi, K. J.; Takeuchi, E. S.; West, A. C. Modeling the Mesoscale Transport of Lithium-Magnetite Electrodes Using Insight from Discharge and Voltage Recovery Experiments. *J.*

Electrochem. Soc. **2015**, *162*, A2817–A2826.

(22) Arora, P. Capacity Fade Mechanisms and Side Reactions in Lithium-Ion Batteries. *J. Electrochem. Soc.* **1998**, *145*, 3647.

(23) Wohlfahrt-Mehrens, M.; Vogler, C.; Garche, J. Aging Mechanisms of Lithium Cathode Materials. *J. Power Sources* **2004**, *127*, 58–64.

(24) Bock, D. C.; Pelliccione, C. J.; Zhang, W.; Wang, J.; Knehr, K. W.; Wang, J.; Wang, F.; West, A. C.; Marschilok, A. C.; Takeuchi, K. J.; Takeuchi, E. S. Dispersion of Nanocrystalline Fe3O4 within Composite Electrodes: Insights on Battery-Related Electrochemistry. *ACS Appl. Mater. Interfaces* **2016**, *8*, 11418–11430.

(25) Ito, S.; Nakaoka, K.; Kawamura, M.; Ui, K.; Fujimoto, K.; Koura, N. Lithium Battery Having a Large Capacity Using Fe3O4 as a Cathode Material. *J. Power Sources* **2005**, *146*, 319–322.

(26) Ramadesigan, V.; Northrop, P. W. C.; De, S.; Santhanagopalan, S.; Braatz, R. D.; Subramanian, V. R. Modeling and Simulation of Lithium-Ion Batteries from a Systems Engineering Perspective. *J. Electrochem. Soc.* **2012**, *159*, R31–R45.

(27) Newman, J.; Thomas-Alyea, K. E. *Electrochemical Systems*, 3rd ed.; John Wiley & Sons, Inc.: Hookben, New Jersey, 2004.

(28) Knehr, K. W.; Cama, C. A.; Brady, N. W.; Marschilok, A. C.; Takeuchi, K. J.; Takeuchi, E. S.; West, A. C. Simulations of Lithium-Magnetite Electrodes Incorporating Phase Change. *Electrochim. Acta* **2017**, *238*, 384–396.

(29) Ohzuku, T.; Uedat, A. Phenomenological Expression of Solid-State Redox Potentials of LiCoO2, LiCo1/2Ni1/202, and LiNiO2 Insertion Electrodes. *J. Electrochem. Soc.* **1997**, *144*, 2780–2785.

(30) Guo, Q.; White, R. E. Cubic Spline Regression for the Open-Circuit Potential Curves of a Lithium-Ion Battery. *J. Electrochem. Soc.* **2004**, *152*, A343–A350.

(31) Karthikeyan, D. K.; Sikha, G.; White, R. E. Thermodynamic Model Development for Lithium Intercalation Electrodes. *J. Power Sources* **2008**, *185*, 1398–1407.

(32) Prausnitz, J. M.; Lichtenthaler, R. N.; Azevedo, E. G. de. *Molecular Thermodynamics of Fluid-*

Phase Equilibria; Pearson Education: Upper Saddle River, New Jersey, 1998.

(33) Walas, S. M. *Phase Equilibria in Chemical Engineering*; Butterworth: Stoneham, Massachusetts, 1985.

(34) Dees, D. W.; Kawauchi, S.; Abraham, D. P.; Prakash, J. Analysis of the Galvanostatic Intermittent Titration Technique (GITT) as Applied to a Lithium-Ion Porous Electrode. *J. Power Sources* **2009**, *189*, 263–268.

(35) Prosini, P.; Lisi, M.; Zane, D.; Pasquali, M. Determination of the Chemical Diffusion Coefficient of Lithium in LiFePO4. *Solid State Ionics* **2002**, *148*, 45–51.

(36) Park, M.; Zhang, X.; Chung, M.; Less, G. B.; Sastry, A. M. A Review of Conduction Phenomena in Li-Ion Batteries. *J. Power Sources* **2010**, *195*, 7904–7929.

(37) Bruggeman, D. A. G. Berechnung Verschiedener Physikalischer Konstanten von Heterogenen Substanzen. I. Dielektrizitätskonstanten Und Leitfähigkeiten Der Mischkörper Aus Isotropen Substanzen. *Ann. Phys.* **1935**, *416*, 636–664.

(38) Tjaden, B.; Cooper, S. J.; Brett, D. J.; Kramer, D.; Shearing, P. R. On the Origin and Application of the Bruggeman Correlation for Analysing Transport Phenomena in Electrochemical Systems. *Curr. Opin. Chem. Eng.* **2016**, *12*, 44–51.

(39) Santos-Carballal, D.; Roldan, A.; Grau-Crespo, R.; de Leeuw, N. H. A DFT Study of the Structures, Stabilities and Redox Behaviour of the Major Surfaces of Magnetite Fe3O4. *Phys. Chem. Chem. Phys.* **2014**, *16*, 21082–21097.

(40) Yang, T.; Wen, X.-D.; Li, Y.-W.; Wang, J.; Jiao, H. Interaction of Alkali Metals with the Fe3O4(111) Surface. *Surf. Sci.* **2009**, *603*, 78–83.

(41) Yu, X.; Li, Y.; Li, Y.-W.; Wang, J.; Jiao, H. DFT+U Study of Molecular and Dissociative Water Adsorptions on the Fe3O4 (110) Surface. *J. Phys. Chem. C* **2013**, *117*, 7648–7655.

(42) Liu, H.; Wang, G.; Wang, J.; Wexler, D. Magnetite/carbon Core-Shell Nanorods as Anode Materials for Lithium-Ion Batteries. *Electrochem. commun.* **2008**, *10*, 1879–1882.

(43) Brady, N. W.; Zhang, Q.; Knehr, K. W.; Liu, P.; Marschilok, A. C.; Takeuchi, K. J.; Takeuchi, E.

S.; West, A. C. Discharge, Relaxation, and Charge Model for the Lithium Trivanadate Electrode: Reactions, Phase Change, and Transport. *J. Electrochem. Soc.* **2016**, *163*, 2890–2898.

Conspectus Figure:

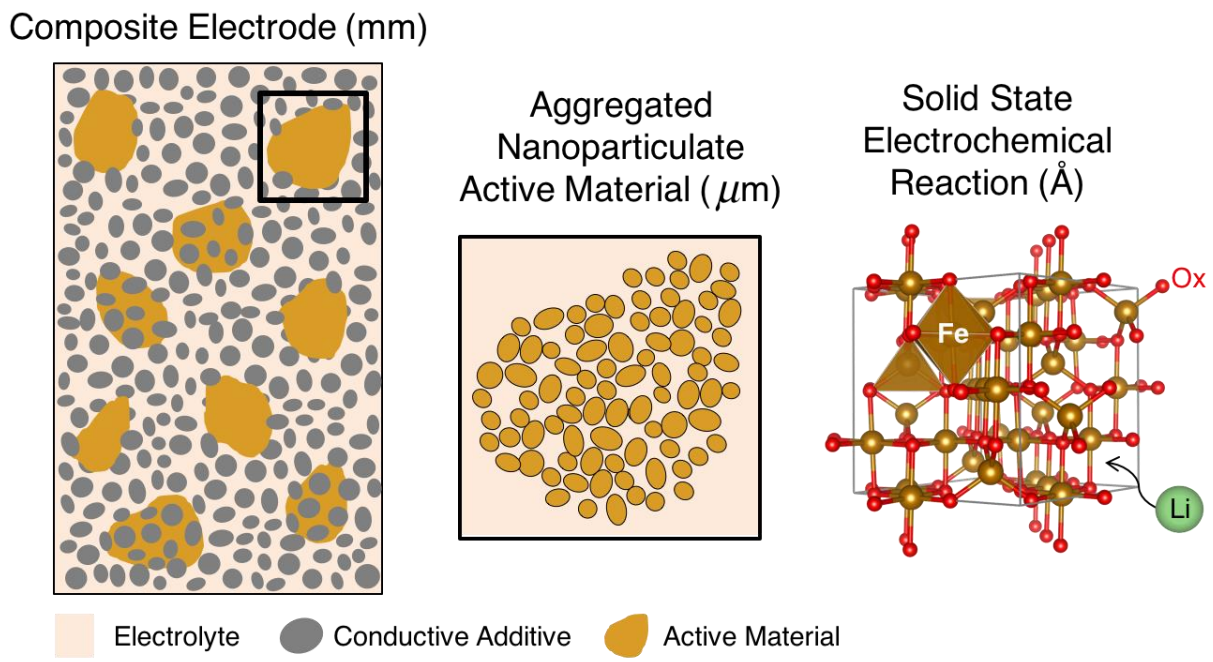

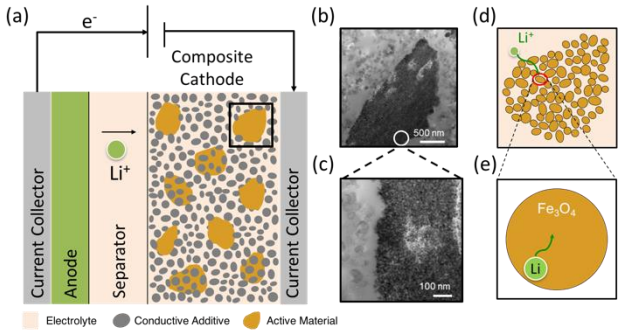

Figure 1. a) Schematic of a lithium-ion battery with Li^0 negative electrode (anode). The positive electrode (cathode) is a composite compised of active material, binder (not shown), and conductive additive. Electron and Li^+ transport shown by arrows for discharge. b) TEM of micron sized agglomerates in Fe_3O_4 electrode[10] and c) magnification of agglomerate, showing nanoparticulate Fe_3O_4.[10] d) Schematic of lithium-ion transport through porous regions between the nanopartictles of an agglomerate and e) solid-state transport of lithium through the nanoparticulate Fe_3O_4.

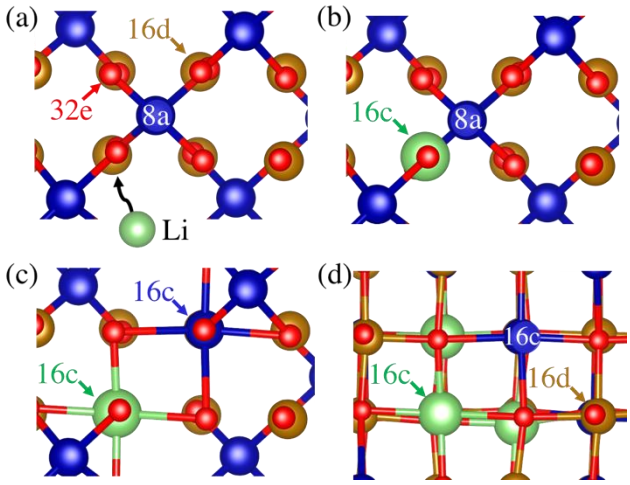

Figure 2. a) Zoom in on Fe_3O_4 with tetrahedral 8a iron in blue, octahedral 16d iron in brown, and 32e oxygen shown in red. Lithium is shown in green. All 16c sites are vacant. b) A structure showing lithium inserting onto a vacant 16c site. c) The resultant Coulombic repulsion from the tetrahedral 8a iron and the inserted 16c lithium causes 8a iron to migrate to a vacant 16c site. d) Full movement of all 8a iron to 16c sites due to Coulombic interactions.

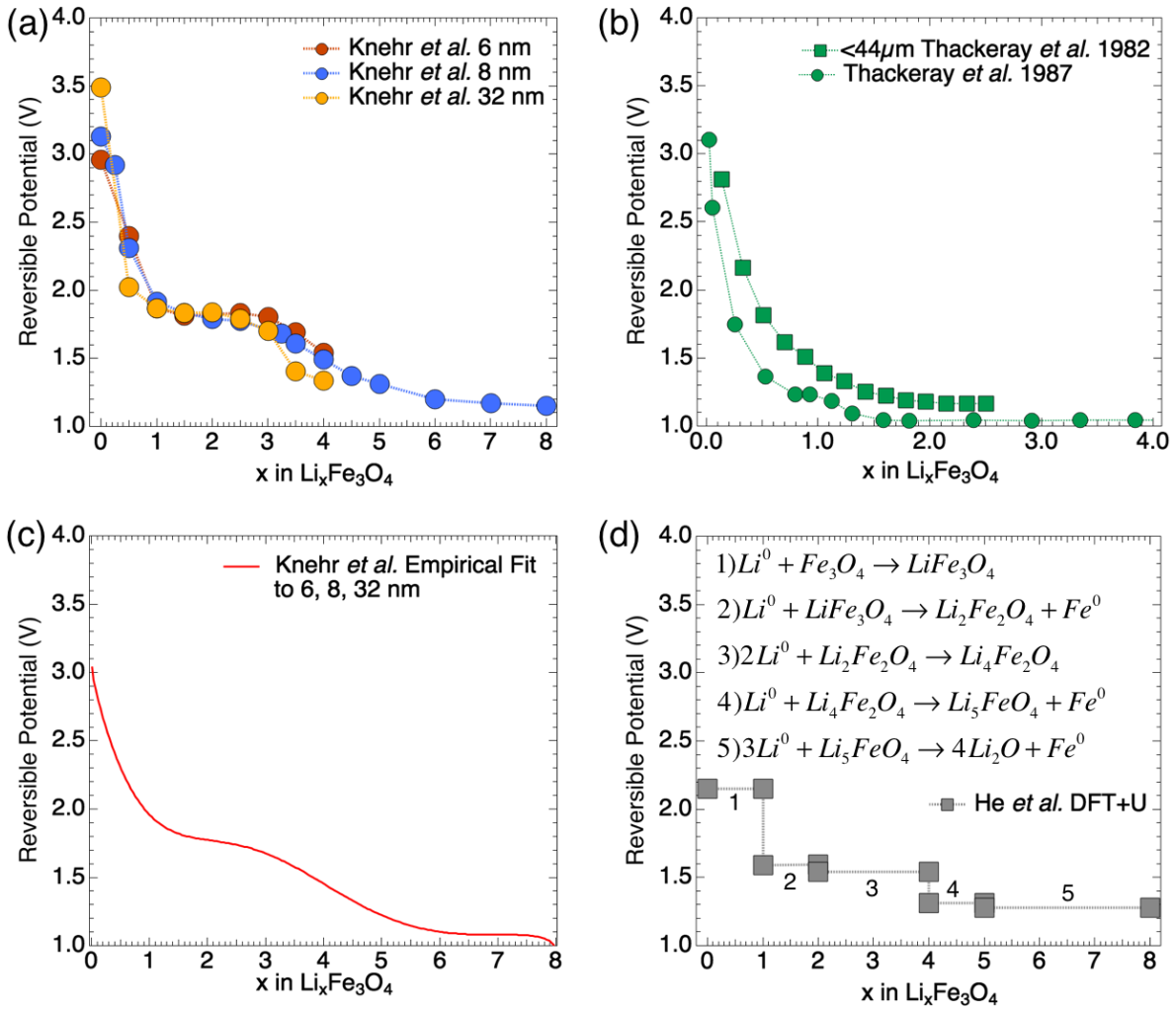

Figure 3. The reversible potential for lithiation of magnetite as reported in the literature. a) GITT experiments of 6, 8, and 32-nm Fe_3O_4.[12,21] b) GITT experiment of <44 micron Fe_3O_4.[3,11] c) Redlich-Kister empirical fit to 6, 8, and 32-nm data in a). [12,21] d) DFT+U determined OCP from He et al.[7]

(a)

	XRD	XANES	EXAFS	STEM	HAAD/ABF
	Bulk information	*Atoms' local environment, coordination number, distance between atoms*		*Atomic resolution imaging, contrast directly related to atomic number*	
x=1.0	Inverse Spinel (0.7)	Fe(8a) Decreasing (0.7)	No Change (0.7)	Fe(8a) → Fe(16c) (0.6)	
x=2.0	Inverse Spinel (1.7)			FeO Peaks	Equal Fe occupation on 16c, 16d (FeO)
x=3.0	Intermediate Structure (2.8)	Fe8a Decreasing (2.8)	10-20% FeO-like (2.8)		
x=4.0	FeO	Fe Oxidation State Change	Single Fe-Fe bond length		No Fe^0, Increased Li on 8a, 48f, 8b
x=6.0			20% Fe^0	Li_2O, FeO, Fe^0 ~1 nm BCC Fe^0 particles	Fe^0/FeO, Presence of nanograins
x=8.0	FeO		50% Fe^0, Single Fe-Fe bond length (FeO)	Li_2O, Fe^0, 1 nm nanograins	Fe^0/FeO More Fe^0 than at 6.0

(b)

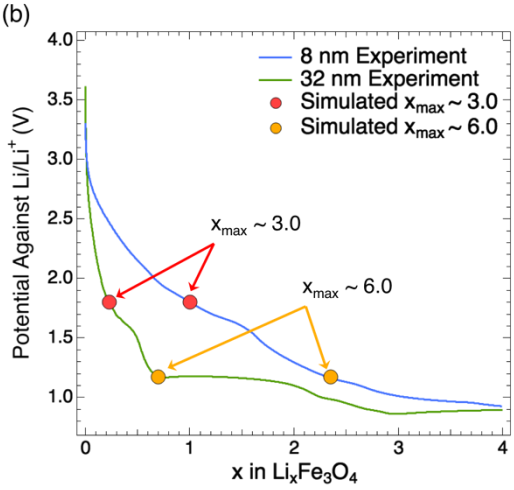

Figure 4. a) Materials characterization results for 9-10.6 nm Fe_3O_4 as a function of x.[1,5] b) Experimental discharge curves at C/200 for 8-nm and 32-nm Fe_3O_4 and mutli-scale simulation predictions for the concentrations of lithium at the surface of the agglomerate, x_{max}.

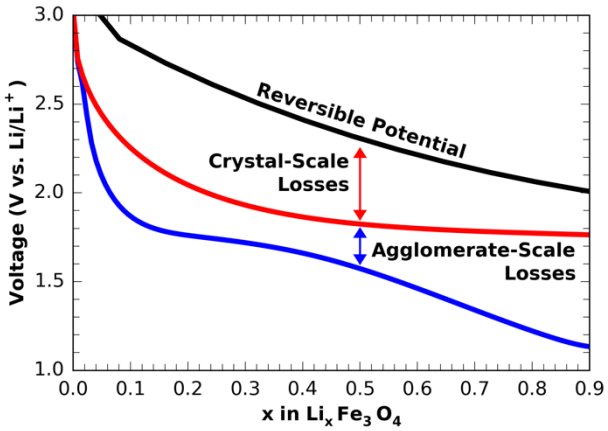

Figure 5. Dissection of the transport resistances occurring within a magnetite electrode discharged at C/200 and composed of 32-nm crystals which form 1.05-μm agglomerates.

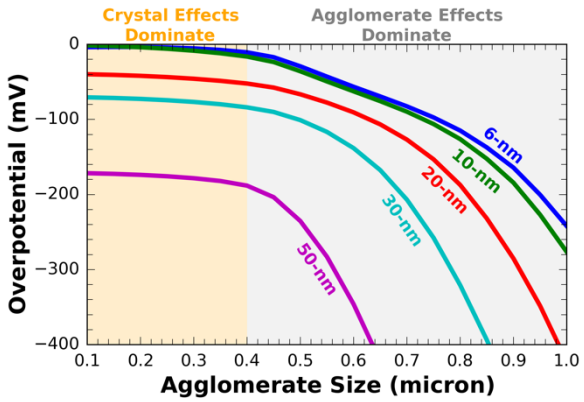

Figure 6. Simulated overpotential predictions for varying crystal sizes and varying agglomerate sizes of magnetite electrodes discharged at C/200 to a composition of $Li_{1.5}Fe_3O_4$.